






## Structural Design Optimization for Unmanned Aircraft Propeller Blades Using the Multi-Objective Colonial Competitive Algorithm

Mohamed Nejlaoui<sup>\*</sup>, Mansour Mohammad Al-Subaihi<sup>†</sup>, Abdullah Falah Alharbi<sup>‡</sup>

Department of Mechanical Engineering, College of Engineering, Qassim University, Buraidah 51452, Saudi Arabia

Corresponding Author Email: [m.nejlaoui@qu.edu.sa](mailto:m.nejlaoui@qu.edu.sa)

Copyright: ©2024 The authors. This article is published by IETA and is licensed under the CC BY 4.0 license (<http://creativecommons.org/licenses/by/4.0/>).

<https://doi.org/10.18280/jesa.570614>

### ABSTRACT

**Received:** 17 October 2024

**Revised:** 26 November 2024

**Accepted:** 6 December 2024

**Available online:** 31 December 2024

#### **Keywords:**

*blade, aircraft, optimization, algorithms, propeller*

The rapid evolution of unmanned technology demands the development of optimized propeller designs that can accommodate a wide range of flight conditions and mission requirements. This article suggests a multi-objective optimization framework for unmanned aircraft during the cruising phase, based on the Multi-Objective Colonial Competitive Method (MOCM). This paper focuses on the maximum thrust-to-weight ratio at hover (T-WHmax) as one of its objective functions, which is associated with the ability to resist wind and maneuver effectively during takeoff and landing. The total energy consumption is the second objective function. Using the suggested framework for the Airbus Vahana unmanned aircraft, the structure of the propeller blade (PB) is optimized and verified through computational fluid dynamics (CFD). A detailed analysis is conducted on the effects of the hover disk loading and cruising speed on the optimization outcome. The findings indicate that T-WHmax greatly influences the outcome of optimization. A comparison with literature results proves the benefits of the optimal PB design in both saving energy and improving takeoff maneuverability. In general, the method and guidelines outlined in this paper endorse the structural optimization of PB design for unmanned aircraft.

## 1. INTRODUCTION

The remarkable advancement of flight control technology has led to a surge of research interest for unmanned aircraft. The two most frequently employed unmanned aircraft, in cargo delivery and urban flight, are tilt-rotor and tilt-wing aircraft [1-6]. The adopt blades in the propellers have a great importance on the unmanned aircraft performances. The clear distinction between vertical flight mode and level flight mode makes blade shape optimization more challenging. During vertical takeoff and landing, a significantly higher quantity of thrust is needed compared to flying at a steady level. However, the ratio of advancement is significantly lower during vertical takeoff and landing [7]. Leishman outlined the constraints of a prop-rotor scheme and stated that as the efficiency of horizontal flight increases, the figure of merit (FIOM) decreases [8]. In terms of energy efficiency, there is an inherent conflict between the two flight modes.

A few studies on optimizing the structure of propeller blades have been carried out. Using the particle swarm optimization (PSO) method and vortex theory, Duan et al. [9] enhance the propeller blade design. The outcome demonstrated the benefits of their proposed design for vertical takeoff and landing. Ciccariello [10] model the chord-length and angle of rotation distribution by using polynomial equations.

A prop-rotor's optimization scheme, based on the blade elements and momentum principle (BEMP), was developed.

Using the Model Center program, Ugwueze et al. [11] developed an optimal design of the PB. Droandi and Gibertini [12] employed the BEMP and genetic algorithm (GA) to enhance the characteristics airfoil distribution of a PB. The aforementioned studies have improved the blade shape research study content. However, none of the aforementioned studies took into account T-WHmax, which is a crucial factor during takeoff and landing. In fact, a higher T-WHmax allows for greater thrust output for controlling attitude [13].

Several research Works have been developed to increase the T-WHmax for multi-rotors [14-16]. In contrast, there are not many studies on tilt-wing, which is significant for Airbus Vahana unmanned aircraft safety [17]. Additionally, Airbus Vahana unmanned aircraft created for quick responses must meet specific requests for the extreme scramble degree during vertical flight, which must be taken into account during the design process [18]. In terms of blade design techniques, Hepperle [19] presented an inverse method for designing a blade structure with minimal energy loss using the Betz theory [20], specifically for situations with a set chord distribution.

This inverse method can be used to quickly hasten the optimization process when applied to Airbus Vahana aircraft propeller design in the cruising stage.

As previously mentioned, various optimization strategies were employed to optimize the Airbus Vahana aircraft propeller. A common limitation of these optimization methods is the difficulty in balancing exploitation (rapid convergence) and exploration (diverse solutions) [20-22]. Increasing

convergence speed often limits the algorithm's ability to explore the entire solution space, leading to reduced diversity and suboptimal results [20-22]. As an alternative, the MOCM offers a promising approach to balance exploration and exploitation [23]. MOCM employs an attraction-repulsion (AR) strategy to dynamically switch between these two phases, enabling efficient and effective optimization of complex engineering problems [23]. To the best of our knowledge, no previous studies have explored the application of MOCM to the optimization of aircraft propeller design.

This article explores an optimization framework for designing the shape of Airbus Vahana aircraft propeller using the MOCM method. The importance of the proposed propeller blade optimal designs has been confirmed through comparison with those available in the literature. The remaining sections of this document are structured in the following manner. Section 2 presents the BEMP, the inverse method for overall propeller development, and a simplified model of a brushless DC (BLDC) motor that was utilized in the following optimization process. Data from wind tunnel tests was used to verify both the BEMP and CFD methods with a three-PBs

NACA 5868-9. In Section 3, an original method, for parameterizing chord distribution and an optimization framework for Airbus Vahana aircraft propeller, is introduced. Section 4 discusses how the proposed framework is used to optimize the PB structure for the Airbus Vahana aircraft. The results of the optimization are provided and analyzed in this discussion. Section 5 investigates the effects of parameters like hover disk loading and the cruising flight speed on optimization. The findings offer a standard guide for designing the PBs for Airbus Vahana aircraft.

## 2. AIRBUS VAHANA AIRCRAFT MODEL

### 2.1 Airbus Vahana aircraft and its flight plan

The standard flight plan of Airbus Vahana aircraft involves hovering (referred to as F1), taking off vertically (F2), moving forward, climbing (F3), flying at a constant speed (F4), descending, moving backward and landing vertically (F5), as illustrated in Figure 1.

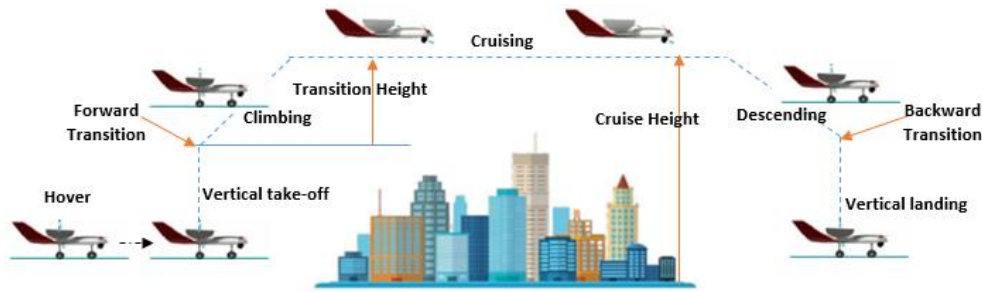


Figure 1. Airbus Vahana aircraft flight profile



Figure 2. Airbus Vahana aircraft structure

Energy consumption is minimal during descent, while time

is restricted for both forward and backward transition flights. Therefore, this paper does not consider these three stages.

The Airbus Vahana aircraft utilizes eight PBs, each with a 1.5 m diameter, for propulsion (Figure 2). The design parameters were determined based on reference [16]. The height for transitioning was established at 100 meters and the vertical takeoff velocity was 3 meters per second. In order to prevent the formation of a vortex ring phenomenon, the vertical landing speed was set at 1.5 meters per second [16].

Table 1 displays the parameters for various flight stages.

In the Airbus aircraft, the PBs are driven by BLDC motors with several characteristics displayed in Table 2.

Table 1. Parameters of flight stages [11, 13]

| Stage          | Hover | Vertical Takeoff | Climbing | Cruising | Vertical Landing |
|----------------|-------|------------------|----------|----------|------------------|
| Symbol         | F1    | F2               | F3       | F4       | F5               |
| Velocity (m/s) | 0     | 3                | 37       | 65.25    | -1.5             |
| Thrust (N)     | 922.4 | 922.4            | 169.4    | 155.8    | 922.4            |
| Time (s)       | 30    | 34               | 124      | 920      | 67               |

Table 2. BLDC motor parameters [13]

| Parameter  | Value  |
|--|--------|
| Maximum of the input power $P_{max}^{in}$ (kW)   | 40     |
| Maximum of revolutionary speed $W_s^{max}$ (rpm) | 5500   |
| Maximum of BLDC output torque $T_o^{max}$ (Nm)   | 200    |
| Range of BLDC input voltage $U^{in}$ (V)         | 24-800 |
| BLDC speed constant $C_s$ (rpm/V)                | 8      |
| BLDC internal resistance $R^{in}$ ( $\Omega$ )   | 0.25   |
| BLDC no-load current $I^N$ (A)                   | 2      |

### 2.2 Momentum concept of blade elements

#### 2.2.1 Theoretical framework

The BEMP uses both the blade element principle (BEP) and momentum principle (MP) to calculate the axial and rotational velocities induced at the propeller blade position. Glauert [24] initially suggested the idea of BEMP. Many studies have confirmed the BEMP's effectiveness in evaluating blade performance.

$$F_{TH} = \underbrace{2\pi D_e r dr |S_0 + S_a| \cdot 2S_a \cdot P}_{MP} = \underbrace{\frac{1}{2} D_e n_B \left[ \frac{|S_0 + S_a|}{\sin \psi} \right]^2}_{BEP} [CL(\mu - \psi) \cos \psi - CD(\mu - \psi) \sin \psi]$$

$$F_T = \underbrace{2\pi D_e r dr |S_0 + S_a| \cdot 2S_t \cdot P}_{MP} = \underbrace{\frac{1}{2} D_e n_B \left[ \frac{|S_0 + S_a|}{\sin \psi} \right]^2}_{BEP} [CL(\mu - \psi) \sin \psi - CD(\mu - \psi) \cos \psi] \quad (1)$$

$$\psi = \arctan \frac{|S_0 + S_a|}{2\pi S_u r - S_t}$$

The force and velocity acting on the blade element, of radius  $r$ , are displayed in Figure 3. Here, the blade element's lift and right drag are represented by  $L$  and  $D$ , its axial thrust and tangential force by  $F_{TH}$  and  $F_T$ , and its twist, angle of attack, interference, and inflow angles by  $\mu$ ,  $\beta$ ,  $\gamma$ , and  $\psi$ .  $S_0$  represents the far-field speed, while  $S_a$  and  $S_t$  indicate the disk axial and tangential speeds.  $S_{tot}$  represents the resultant speed while  $S_u$  is the rotational speed in rpm.

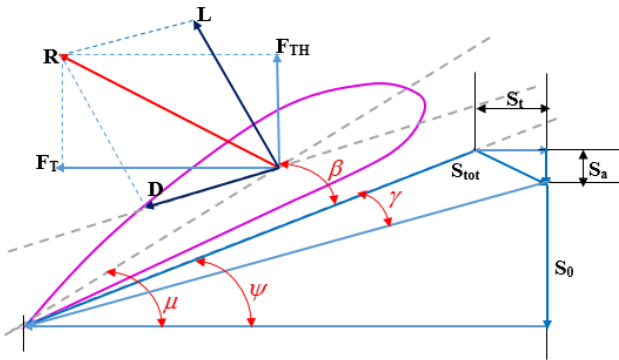


Figure 3. The speed and forces applied to the blade part

Eq. (1) can be used to determine the axial thrust and tangential force while considering the Prandtl adjustment [13].

The Prandtl modification factor  $P$  is determined using:

$$P = \frac{2}{\pi} \arccos(e^{-m}), m = \frac{n_b}{2} \frac{Di - r}{r \sin \psi_t} \quad (2)$$

where,  $n_b$ ,  $Di$  and  $D_e$  are the blade number, diameter and material density, respectively.  $CL$  and  $CD$  are lift and drag aerodynamic coefficients.  $\psi_t$  represents the current inflow angle at the tip of the blade. Eq. (1) is a non-linear; Liu et al. [16] proposed an iterative method based on gradients, utilizing an unknown variable  $\beta$  for solution.

### 2.2.2 2D Airfoil aerodynamics model

The propeller sections' airfoils were derived from transforming a Clark Y airfoil [16] using an affine transformation. The BEMP is directly affected by the precision of 2D airfoil aerodynamics. Three key factors that affect the 2D aerodynamics of a particular airfoil are the Reynolds number, mach number, and angle of attack. Moreover, unlike traditional propeller design and optimization, an Airbus Vahana aircraft propeller often experiences high angle of attack flow near the root of the propeller when operating at low advance ratios.

The Latin hypercube sampling (LHS) technique [25] was utilized for sampling the angle of attack ( $\beta = -10$  to  $75^\circ$ ), Reynolds numbers ( $5 \times 10^4$  to  $3 \times 10^6$ ), airfoil thicknesses ( $At = 0.03$  to  $0.4$ ), and Mach numbers ( $Mn = 0.1$  to  $0.7$ ).

To balance computational cost and statistical precision, 80 LHS samples were used. This number consistent with the recommendations of prior research for LHS-based UAV propeller blade design [9-13]. The database was produced through 2D CFD simulations utilizing structural grids (Figure 4) and the Spalart-Allmaras (S-A) turbulence model [26] to calculate  $CL$  ( $\beta$ ,  $Mn$ ,  $Re$ ,  $At$ ) and  $CD$  ( $\beta$ ,  $Mn$ ,  $Re$ ,  $At$ ).

A Backpropagation Artificial Neural Network (BP-ANN) with one input layer, one hidden layer, and one output layer was trained using Bayesian regulation on the airfoil aerodynamic database. The BP-ANN received  $\beta$ ,  $Mn$ ,  $Re$ ,  $At$  as inputs and produced  $CL$  and  $CD$  as outputs. After making various changes, the hidden layer was determined to have 13 neurons.

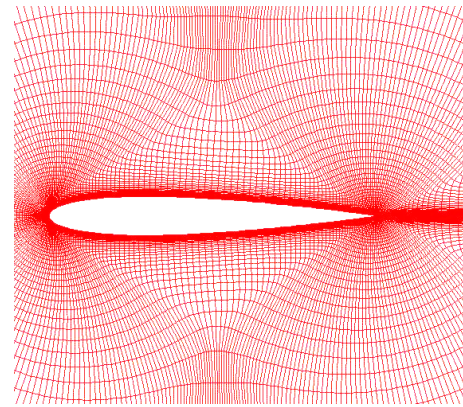
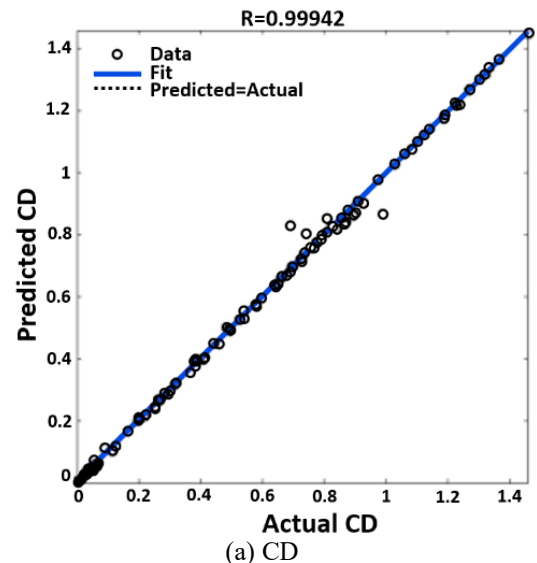


Figure 4. The airfoil grid used in 2D CFD simulation

Figure 5 displays the regression results of the trained BP-ANN surrogate model. The training result showed a mean squared error of  $2.63 \times 10^{-4}$ , confirming the accuracy of the BP-ANN surrogate model.



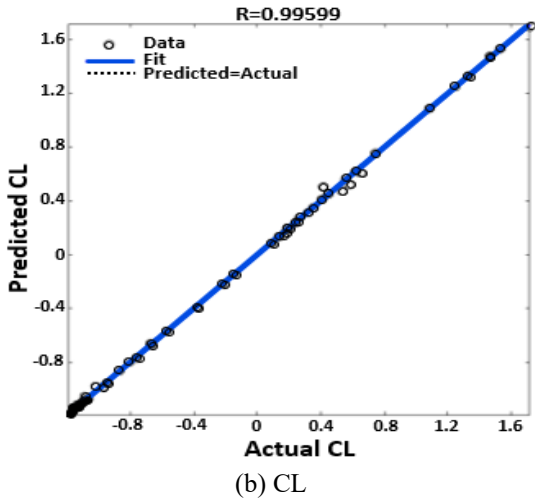


Figure 5. BP-ANN regression for 2D airfoil aerodynamics

### 2.3 Inverse design method for propeller in cruise phase

For Airbus Vahana aircraft, the primary mode of energy consumption is the level flying mode, which comprises cruising and rising [19]. The inverse design method based on the Betz optimum theory was utilized to the cruising stage to attain maximum energy efficiency in level flight [27].

In order to achieve the optimal PB with minimal energy losses, the axial displacement velocity ratio ( $\xi$ ) should remain constant across the radius. However, the value of  $\xi$  is unidentified [27]. By combining the Betz optimum theory with BEMP, a 3~4 numerical iterations process can lead to acquiring an optimal propeller, as stated in reference [27]. This approach is called the regular design method. The input for this regular approach is a local lift coefficient that corresponds to the highest lift-drag ratio along the radius. In reality, the numerical iterative method makes it simple to derive the remaining two distribution rules in terms of the aerodynamic coefficients, chord-length, and twist angle distribution, once one of them is prescribed. Therefore, for a propeller with a specified chord length distribution ( $C_h$ ), Hepperle [19] suggested an inverse design approach. Figure 6 displays the inverse design strategies.

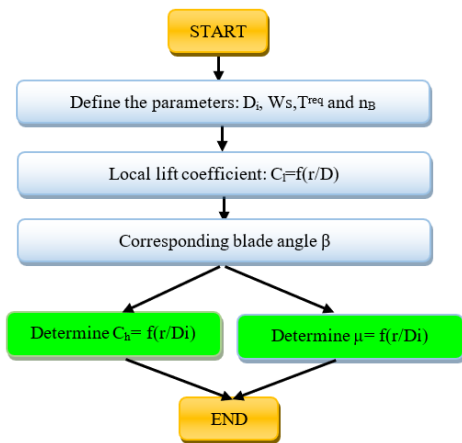


Figure 6. The inverse design method

By using this inverse technique, the propeller optimization framework's cruising stage may automatically produce a minimum energy loss propeller, saving the effort of parameterizing the twist angle distribution. Parameterizing  $C_h$

distribution allows a more intuitive way to establish physical constrictions by restricting the minimum  $C_h$ , resulting in fewer infeasible designs initially compared to parameterizing the lift coefficients.

### 2.4 Model of the DC motor

BLDC motors are commonly utilized in Airbus Vahana aircraft due to their high efficiency and substantial torque. In this study, assuming negligible conductors, iron and mechanical losses. In fact, these losses can be relatively small compared to other losses, such as copper losses [10-12].

A first-order energy model of a BLDC motor was utilized for determining power and energy values. In each flight stage  $F_i (i = 1\sim 5)$ , the BLDC motor's revolutionary speed  $W_s$ , output torque ( $T_o$ ), and efficiency  $E_m$  have a correlation as indicated in reference [28].

$$\begin{aligned}
 I_i &= \frac{2\pi C_s T_o}{60} + I^N \\
 U^{in} &= \frac{60 W_s}{2\pi C_s} + I_i R^{in} \\
 E_m &= \frac{2\pi T_o}{60 U^{in} I_i}
 \end{aligned} \tag{3}$$

The power absorbed by the propeller at state ( $i$ ) is given as  $P^P$ , and  $P^{in}$  is the BLDC's input power, which is determined by:

$$P^{in} = \frac{P^P}{E_m} \tag{4}$$

The three defining parameters of a BLDC motor are the internal resistance ( $R^{in}$ ), no-load current ( $I^N$ ), and speed constant ( $C_s$ ). The input voltage and closed-circuit current are denoted by  $U^{in}$  and  $I$ , respectively.

### 2.5 Non-cruising stage trimming

Solving the trimming of revolutionary speed and/or collective pitch during non-cruising stages such as hover and takeoff is necessary in order to optimize energy consumption for the entire mission profile. The trimming process involves solving a minimum power optimization problem using the rotational speed ( $W_s$ ) and collective pitch ( $d\mu$ ) as the design parameters.

$$\text{Minimize } P^{in}(W_s, d\mu) \tag{5}$$

The second goal is to achieve  $T-WH_{max}$  while hovering at F1, as shown by the following expression:

$$T - WH_{max} = \frac{n_p T_1^{max}}{\omega_{ov} g} \tag{6}$$

In the previous equation,  $g$  is the acceleration due to gravity,  $\omega_{ov}$  is the total takeoff weight, and  $n_p$  is the number of propellers. At the same time, in order to finish the vertical flight stage F5 at maximum velocity, the maximum thrust in F5 needs to meet the following criterion:

$$n_p T_5^{max} \geq \omega_{ov} g \tag{7}$$



### 3. OPTIMIZATION PROBLEM AND STRATEGY

#### 3.1 Optimization problem

Using a suitable parametric approach for the chord length distribution ( $C_h$ ) can reduce the occurrence of impractical designs in the design variables ( $DVs$ ) generation process. A piecewise quadratic polynomial method [28] was utilized in this section. In fact, the chord-length at point o was determined as  $C_h = (pa+1) C_{hlin}$  with a given parameter  $pa$ .  $C_{hlin}$  is the virtual linear short length of a point O given by:

$$C_{hlin} = \frac{C_{tip} - C_{root}}{\frac{Di}{2} - R_h} (r_{lon} - R_h) + C_{root} \quad (8)$$

where,  $r_{lon}$  represents the longitudinal position of point O.  $R_h$  represents the hub's radius, while  $C_{root}$  and  $C_{tip}$  indicate the chord length at the propeller's root and tip, respectively.  $Di$  defines the diameter of the blade. Figure 7 illustrates more details about the used piecewise quadratic polynomial method.

The time designated for each stage of the flight was indicated as  $t^i$  ( $i=1,2,\dots,5$ ) and the total energy used in the entire mission profile was given by:

$$E_{MP} = \sum_{i=1}^5 P_i^{in} t^i \quad (9)$$

The optimization issue can be formulated as:

$$\begin{cases} \text{Minimize} & E_{MP} = \sum_{i=1}^5 P_i^{in} t^i \\ \text{Maximize} & T - WH_{max} = \frac{n_p T_1^{max}}{\omega_{ov} g} \end{cases} \quad (10)$$

Under constraints  $\begin{cases} n_p T_5^{max} \geq \omega_{ov} g \\ DVs \in RA \end{cases}$

The design variables ( $DVs$ ) for the blade propeller optimization problem were outlined with their respective ranges ( $RA$ ) in Table 3. In this table  $W_{S4}$  note the angular speed at F4 stage. The MOCM method will be used to solve Eq. (10).

**Table 3.** Parameters of flight stages [13, 16]

| DV             | RA          |
|----------------|-------------|
| $C_{root}$ (m) | [0.075 0.2] |
| $C_{tip}$ (m)  | [0.04 0.12] |
| $pa$           | [0 2]       |
| $r_{lon}$ (m)  | [0.2R 0.7R] |
| $W_{S4}$ (rpm) | [1000 3300] |

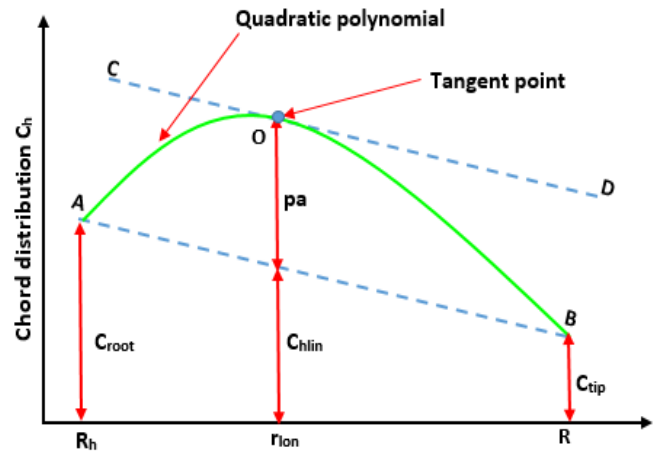


**Figure 7.** Picewise quadratic polynomial method

#### 3.2 MOCM optimization method

Recently, Bilel et al. [23] developed a stochastic MOCM that was influenced by imperialist competition. This algorithm integrates the attraction and repulsion operators in order to obtain the best compromise between convergence and diversity. These operators are guaranteed by the multi-points crossover and the random replacement mutation concepts [23].

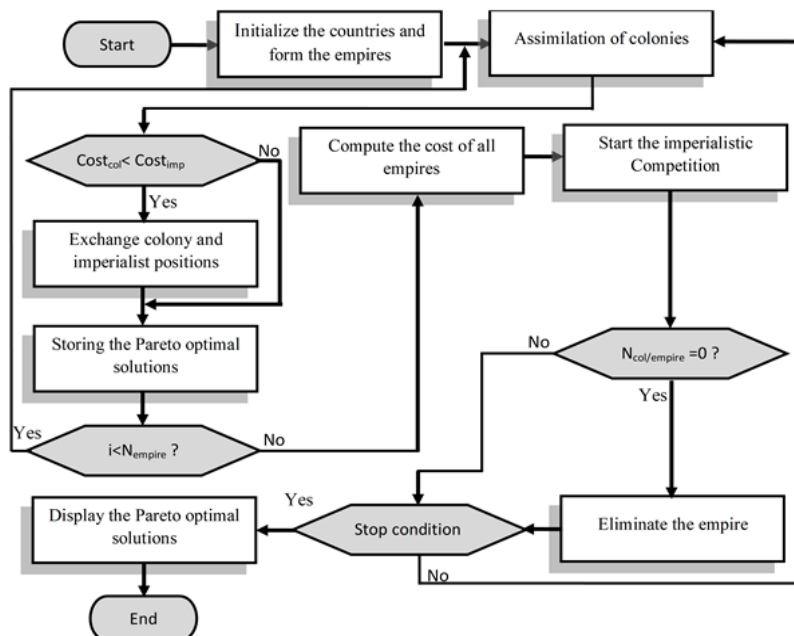


**Figure 8.** The MOCM flowchart

Moreover, the fast non-dominated sorting approach is used to find the non-dominated solutions forming the Pareto front. Figure 8 shows the flowchart of the MOCM. The MOCM begins with a generation of an initial population randomly. Each element of the population is a country. The most powerful country is called “imperialist”. The remaining countries are considered as “colonies”.

Due to imperialists’ powers, the colonies of the initial population are divided among them to form the initial empires. Each initial empire is composed of one imperialist and several colonies. After forming the initial empires, the colonies start

moving towards their relevant powerful imperialist. During the imperialists competition all empires, based on their power, try to acquire the weakest colonies of other weak empires. The weakest empires lose their colonies and collapse. The MOCM algorithm stops when all the weak empires collapse except the powerful one [23].

The MOCM method will be integrate in the general optimization framework presented in Figure 9. The green block presents the MOCM method utilized to solve optimization problem (defined by Eq. (10)).

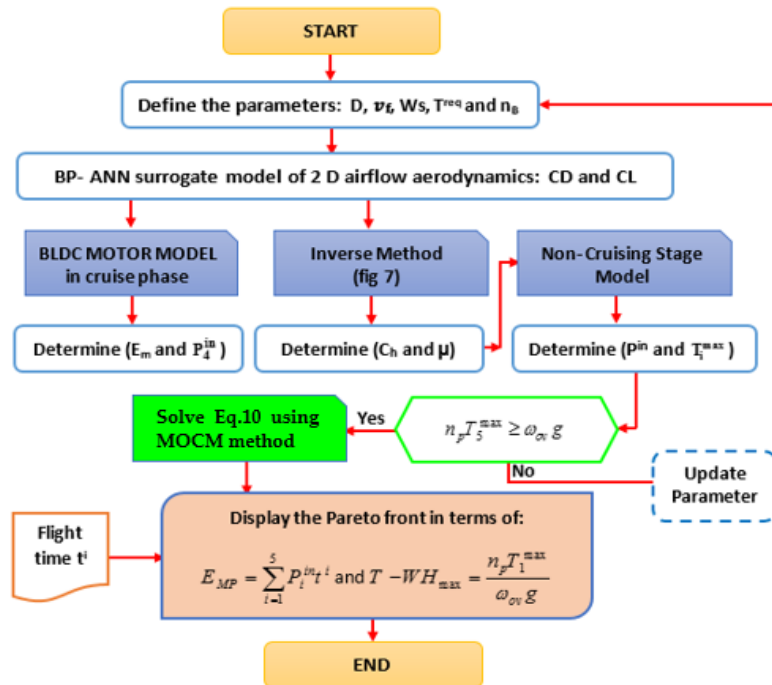


Figure 9. The optimization framework's flow chart

### 3.3 Results of optimization

The Pareto-optimal front is depicted in Figure 10. The Pareto front's sensitivity to MOCM hyper-parameters, such as population size and mutation rate, was assessed through 10 runs with varying parameter settings. It is noted that the overall shape and trend of the Pareto front remained relatively consistent. This proves that the MOCM algorithm is robust to hyper-parameter settings variations.

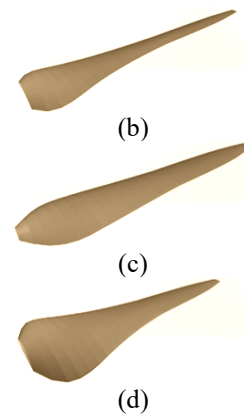
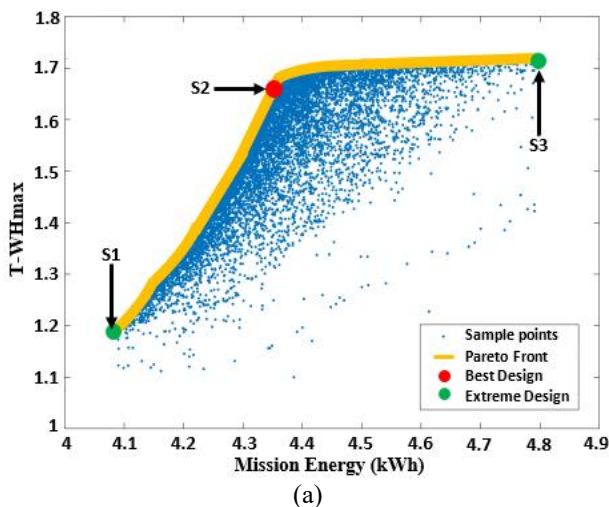


Figure 10. Optimization results: (a) pareto front, (b) S1 design, (c) S2 design, (d) S3 design

One can note the contradiction between the mission energy ( $E_{MP}$ ) and  $T-WH_{max}$ . In fact, a more maneuverable tilt-wing at hover will have lower energy efficiency. The obtained optimal solutions are presented as Pareto front (yellow color in Figure 10). Moreover, other dominated solutions are illustrated, in Figure 10, with blue color.

For more details, Figure 10 illustrates also two extreme solutions S1 and S3 and the optimal solution S2. S1 is the most efficient solution providing the minimum energy

consumption. S3 is the most maneuverable solution offering the  $T-WH_{max}$ . The best compromise between  $E_{MP}$  and  $T-WH_{max}$  is given by S2. Since it offers the best compromise between  $E_{MP}$  and  $T-WH_{max}$ , S2 is considered as the best optimal design. The three-structural shapes of the chosen S1, S2 and S3 solutions are also presented in Figure 10.

The best optimal S2 solution had a  $T-WH_{max}$  of 1.65 at hover and consumed 4.36 kWh of energy. For more details, Figure 11 illustrates the chord length and the twist angle distributions of the chosen best optimal solution (S2).

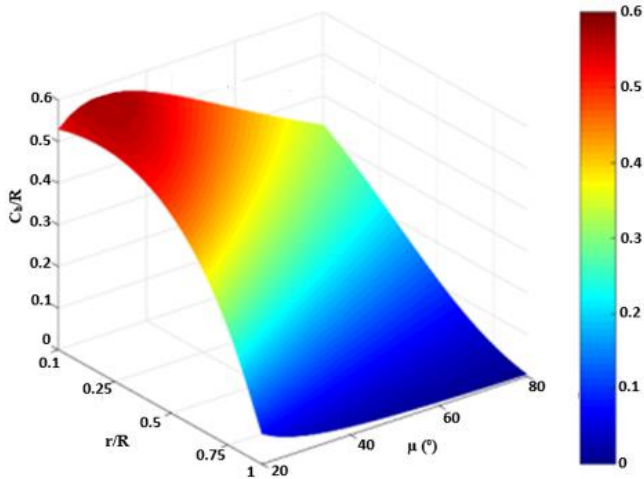


Figure 11. Chord-length and twist angle distribution of S2 solution

To compare the twist and chord length distributions of S2 with S1, and S3 solutions, the average twist amplitude is defined by the following expression [7]:

$$\bar{\mu} = \int_{R_h}^R \frac{d\mu}{d\left(\frac{r}{R}\right)} dr \quad (11)$$

The average blade chord length distribution is given by [7]:

$$\bar{C}_h = \int_{R_h}^R C_h dr \quad (12)$$

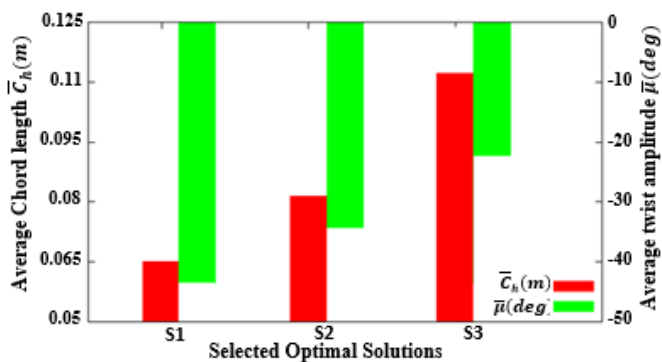


Figure 12. Evolution of  $C_h$  and  $\mu$

Figure 12 displays the average values of  $C_h$  and  $\mu$  for various optimal PBs solutions (S1, S2 and S3). It is clear that, the tilt-wing was more maneuverable during takeoff when the propeller blade was wider. Conversely, a narrower average blade is necessary for achieving higher energy efficiency. In

terms of twist distribution, a lower value of  $\mu$  results in increased maneuverability for the tilt-wing.

### 3.3.1 Analysis of hover disk loading

The propeller's disk loading is the most crucial parameter for the takeoff performance. Figure 13 displays the Pareto-optimal front of the PBs design with varying hover disk loadings. One can note that  $T-WH_{max}$  drops from 1.72 to 1.37 by 25.5% due to an increase in hover disk loading. The lowest  $E_{MP}$  dropped to 4.02 kWh from 4.04 kWh before rising to 4.24 kWh. The minimum mission energy showed a relative variation of less than 5% at its maximum level. In general, the range of hover disk loading had a noticeable effect on the  $T-WH_{max}$ , but only a minimal effect on  $E_{MP}$ . Thus, to enhance the takeoff maneuverability of the Airbus Vahana aircraft used for manned flights in urban areas, it is important to keep the disk loading at a minimum.

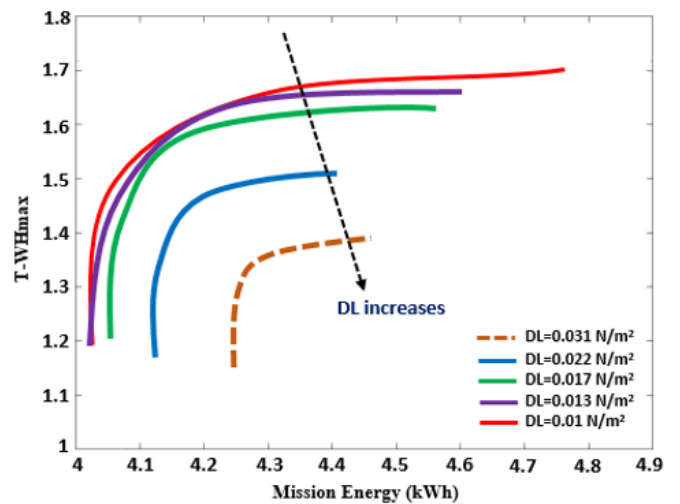


Figure 13. Optimal results with various DL

### 3.3.2 Analysis of the cruising speed

The speed at which a plane cruises ( $Sc$ ) is a crucial factor that affects the flow conditions during level flight. We modified the cruise speed and performed the optimization of the PB again. The obtained results are presented in Figure 14. One can note that an increase in the cruising speed resulted in minimal differences in  $T-WH_{max}$  and a slight increase in the  $E_{MP}$  of the PB design. Thus, the PB design showed lower sensitivity towards the cruising speed.

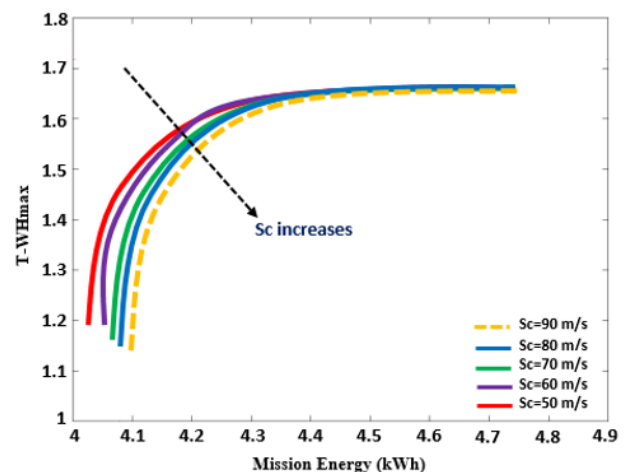


Figure 14. Optimal results with various  $Sc$

### 3.3.3 Comparison with literature results

The obtained optimal results have been compared with those obtained in literature [9, 11, 13]. The comparison has been conducted in terms of the  $E_{MP}$  and the  $T-WH_{max}$ . The comparison results are presented in Table 4.

**Table 4.** Comparison results

| Performances                      | Mission Energy (kWh) | T-WH <sub>max</sub> |
|-----------------------------------|----------------------|---------------------|
| Xia et al. [13]                   | 4.39                 | 1.577               |
| Duan et al. [9]                   | 5.33                 | 1.545               |
| Ugwueze et al. [11]               | 5.82                 | --                  |
| This work                         | 4.082                | 1.735               |
| Maximum Percentage of improvement | 42.6%                | 10.98%              |

One can note that the obtained optimal results present an improvement percentage until 42.6% in terms profile mission energy and 11% in terms of  $T-WH_{max}$ . This emphasizes the importance of the used MOCM method and the optimization framework suggested in this study.

## 4. CONCLUSIONS

In this study, MOCM was effectively incorporated into the optimization framework for Airbus propellers, functioning across a broad spectrum of operating conditions. The suggested framework for optimizing Airbus propellers selected  $T-WH_{max}$  and  $E_{MP}$  as the two main objective functions. The relationship between the  $T-WH_{max}$  and the  $E_{MP}$  efficiency was contradictory.  $T-WH_{max}$  may not always be achieved with minimal hover power. This highlights the importance of considering  $T-WH_{max}$  as a key factor in achieving maneuverability or agility during vertical flight.

An optimal PB design was achieved for Airbus Vahana aircraft within specific BLDC power and torque limitations. Utilizing optimal PB design can lead to a 42.6% energy savings and a 11% increase in  $T-WH_{max}$  compared to literature studies.

Disk loading had a more significant effect on  $T-WH_{max}$  compared to  $E_{MP}$ . It is important for an Airbus aircraft to have low disk loading at hover in order to guarantee sufficient reliability and maneuverability during takeoff and landing. Moreover, the aircraft experienced a slight increase in its minimum energy with a higher cruising speed, while  $T-WH_{max}$  remained relatively unchanged.

The optimal obtained results have been compared with literature findings. The benefits of the optimal PB design have been confirmed, in both saving energy and improving takeoff maneuverability.

## ACKNOWLEDGEMENTS

The authors gratefully acknowledge Qassim University, represented by the Deanship of Graduate Studies and Scientific Research, and Prince Sultan Defense Studies and Research Center for the financial support of this project (PID-000062\_09\_03) during the academic year 1445 AH / 2023 AD.

## REFERENCES

- [1] Gu, H., Lyu, X., Li, Z., Shen, S., Zhang, F. (2017). Development and experimental verification of a hybrid vertical take-off and landing (VTOL) unmanned aerial vehicle (UAV). In 2017 International Conference on Unmanned Aircraft Systems (ICUAS), Miami, FL, USA, pp. 160-169. <https://doi.org/10.1109/ICUAS.2017.7991420>
- [2] Czyba, R., Lemanowicz, M., Gorol, Z., Kudala, T. (2018). Construction prototyping, flight dynamics modeling, and aerodynamic analysis of hybrid VTOL unmanned aircraft. *Journal of Advanced Transportation*, 2018(1): 7040531. <https://doi.org/10.1155/2018/7040531>
- [3] Dündar, Ö., Bilici, M., Ünler, T. (2020). Design and performance analyses of a fixed wing battery VTOL UAV. *Engineering Science and Technology, an International Journal*, 23(5): 1182-1193. <https://doi.org/10.1016/j.jestch.2020.02.002>
- [4] Hadi, G.S., Kusnaedi, M.R., Dewi, P., Budiarto, A., Budiyo, A. (2016). Design of avionics system and control scenario of small hybrid vertical take-off and landing (VTOL) UAV. *Journal of Instrumentation, Automation and Systems*, 2(2): 66-71.
- [5] Botero, E.M., Alonso, J.J. (2017). Conceptual design and optimization of small transitioning UAVs using SUAVE. In 18th AIAA/ISSMO Multidisciplinary Analysis and Optimization Conference, Denver, Colorado, p. 4149. <https://doi.org/10.2514/6.2017-4149>
- [6] Clarke, M., Smart, J., Botero, E.M., Maier, W., Alonso, J.J. (2019). Strategies for posing a well-defined problem for urban air mobility vehicles. In AIAA Scitech 2019 Forum, San Diego, California, p. 0818. <https://doi.org/10.2514/6.2019-0818>
- [7] Qiao, N., Ma, T., Fu, J., Zhang, L., Wang, X., Xue, P. (2023). Rapid blade shape optimization for contra-rotating propellers for eVTOL aircraft considering the aerodynamic interference. *Aerospace*, 10(1): 54. <https://doi.org/10.3390/aerospace10010054>
- [8] Leishman, J.G., Rosen, K.M. (2011). Challenges in the aerodynamic optimization of high-efficiency propellers. *Journal of the American Helicopter Society*, 56(1): 12004-12004. <https://doi.org/10.4050/JAHS.56.012004>
- [9] Duan, D., Wang, Z., Wang, Q., Li, J. (2020). Research on integrated optimization design method of high-efficiency motor propeller system for UAVs with multi-states. *IEEE Access*, 8: 165432-165443. <https://doi.org/10.1109/ACCESS.2020.3014411>
- [10] Ciccariello, S. (2020). The chord-length distribution of a polyhedron. *Acta Crystallographica Section A: Foundations and Advances*, 76(4): 474-488. <https://doi.org/10.1107/S2053273320004519>
- [11] Ugwueze, O., Statheros, T., Horri, N., Bromfield, M.A., Simo, J. (2023). An efficient and robust sizing method for eVTOL aircraft configurations in conceptual design. *Aerospace*, 10(3): 311. <https://doi.org/10.3390/aerospace10030311>
- [12] Droandi, G., Gibertini, G. (2015). Aerodynamic blade design with multi-objective optimization for a tiltrotor aircraft. *Aircraft Engineering and Aerospace Technology: An International Journal*, 87(1): 19-29. <https://doi.org/10.1108/AEAT-01-2013-0005>
- [13] Xia, X., Ma, D., Zhang, L., Liu, X.A., Cong, K. (2022).



- Blade shape optimization and analysis of a propeller for VTOL based on an inverse method. *Applied Sciences*, 12(7): 3694. <https://doi.org/10.3390/app12073694>
- [14] Benini, E. (2004). Significance of blade element theory in performance prediction of marine propellers. *Ocean Engineering*, 31(8-9): 957-974. <https://doi.org/10.1016/j.oceaneng.2003.12.001>
- [15] Xu, J., Yu, J., Lu, X., Long, Z., Xu, Y., Sun, H. (2024). Aerodynamic performance and numerical analysis of the coaxial contra-rotating propeller lift system in Evtol vehicles. *Mathematics*, 12(7): 1056. <https://doi.org/10.3390/math12071056>
- [16] Liu, X., Zhao, D., Oo, N.L. (2023). Comparison studies on aerodynamic performances of a rotating propeller for small-size UAVs. *Aerospace Science and Technology*, 133: 108148. <https://doi.org/10.1016/j.ast.2023.108148>
- [17] Fakhraian, E., Semanjski, I., Semanjski, S., Aghezaf, E.H. (2023). Towards safe and efficient unmanned aircraft system operations: Literature review of digital twins' applications and European Union regulatory compliance. *Drones*, 7(7): 478. <https://doi.org/10.3390/drones7070478>
- [18] Kakavitsas, N., Willis, A., Conrad, J. M., Wolek, A. (2024). Comparison of size and performance of small vertical and short takeoff and landing UAS. In 2024 IEEE Aerospace Conference, Big Sky, MT, USA, pp. 1-14. <https://doi.org/10.1109/AERO58975.2024.10521006>
- [19] Hepperle, M. (2010). Inverse aerodynamic design procedure for propellers having a prescribed chord-length distribution. *Journal of Aircraft*, 47(6): 1867-1872. <https://doi.org/10.2514/1.46535>
- [20] Nejlaoui, M. (2023). Multi-objective enhanced imperialistic competitive method for multi-criteria engineering issues. *International Journal of Computer Applications in Technology*, 69(4): 344-356. <https://doi.org/10.1504/IJCAT.2022.129384>
- [21] Mohamed, N., Bilel, N., Alsagri, A.S. (2020). A multi-objective methodology for multi-criteria engineering design. *Applied Soft Computing*, 91: 106204. <https://doi.org/10.1016/j.asoc.2020.106204>
- [22] Bilel, N., Mohamed, N., Zouhaier, A., Lotfi, R. (2016). An improved imperialist competitive algorithm for multi-objective optimization. *Engineering Optimization*, 48(11): 1823-1844. <https://doi.org/10.1080/0305215X.2016.1141204>
- [23] Bilel, N., Mohamed, N., Zouhaier, A., Lotfi, R. (2019). An efficient evolutionary algorithm for engineering design problems. *Soft Computing*, 23: 6197-6213. <https://doi.org/10.1007/s00500-018-3273-z>
- [24] Glauert, H. (1983). *The Elements of Aerofoil and Airscrew Theory*. Cambridge University Press.
- [25] Phromphan, P., Suvisuthikasame, J., Kaewmongkol, M., Chanpichitwanich, W., Slesongsom, S. (2024). A new Latin hypercube sampling with maximum diversity factor for reliability-based design optimization of HLM. *Symmetry*, 16(7): 901. <https://doi.org/10.3390/sym16070901>
- [26] Kostić, Č. (2015). Review of the Spalart-Allmaras turbulence model and its modifications to three-dimensional supersonic configurations. *Scientific Technical Review*, 65(1): 43-49.
- [27] Ghișescu, M.I., Ghișescu, M., Modrea, A. (2020). A new light aircraft and its design method. *Proceedings*, 63(1): 66. <https://doi.org/10.3390/proceedings2020063066>
- [28] Guibert, V., Condomines, J.P., Brunot, M., Bronz, M. (2021). Piecewise polynomial model identification using constrained least squares for UAS stall. *IFAC-PapersOnLine*, 54(7): 493-498. <https://doi.org/10.1016/j.ifacol.2021.08.408>